Radiation Physics and Chemistry 172 (2020) 108728

Contents lists available at ScienceDirect

Radiation Physics and Chemistry

journal homepage: www.elsevier.com/locate/radphyschem

Dosimetric characterization of 3D printed phantoms at different infill percentages for diagnostic X-ray energy range

D. Villani*, O. Rodrigues Jr., L.L. Campos

Instituto de Pesquisas Energéticas e Nucleares, IPEN/CNEN, USP, Avenida Prof. Lineu Prestes, 2242, Cidade Universitária, São Paulo, SP, 005508-000, Brazil

ARTICLE INFO

Keywords:
3D printing
3D printed phantom
PLA
ABS
Dosimetry

ABSTRACT

The aim of this paper is to characterize 3D printed phantoms and printing set-ups with different infill percentages for imaging energy X-ray beams attenuation. 3D printing performance was studied using the fused filament fabrication (FFF) technique with PLA (Polylactic Acid) and ABS (Acrylonitrile Butadiene Styrene) filaments. Phantom plates were printed and, using the Pantak Seifert X-ray system with different beam qualities in the diagnostic range, the attenuation coefficients were obtained experimentally with the transmission method and results compared with PMMA used as reference and theoretical data. Different percentages of infill of printed phantoms were also evaluated and transmission characterized. The attenuation coefficients were determined for the different beam qualities and results show that the variation in the values of attenuation coefficients decreases as the infill quality increases. Attenuation characteristics evaluated indicates the suitable equivalence of PLA to PMMA for 3D printing water/tissue equivalent most complex geometry phantoms. The different printing modes characterized together with their attenuation coefficients for the X-ray beams will be studied and used in the development of new 3D printed phantoms in our institute.

1. Introduction

Phantoms have become popular and are used in all aspects of medical physics applications. Water-based phantoms exist to measure the output of megavoltage therapy beams and anthropomorphic phantoms can be used to test the ability of the megavoltage beams to accurately deliver a radiotherapy treatment. Imaging phantoms have been designed to be used in the imaging quality assurance of radiation diagnostic techniques. Similar phantoms exist to test the same properties of ultrasound (US), computed tomography (CT), magnetic resonance imaging (MRI), and positron emission tomography (PET) systems (Dewerd, 2014).

Consequentially, the materials within a phantom are often intended to simulate human tissue. However, the properties of these materials vary with the energy of the incident radiation. Thus, while something may be tissue equivalent over a given energy range, it may not be tissue equivalent over all energies (Dewerd, 2014). According to the International Atomic Energy Agency (IAEA) in its Technical Report Series No. 457 (TRS 457), standard phantoms "*should be designed and constructed so that they offer the same primary attenuation and scatter production as the relevant body section(s) of a representative patient*" (International Atomic Energy Agency, 2007). Following this recommendation, the radiation type, quality and the energy range on measurements should also be concerned. Other important characteristics to be considered when building a phantom are the material cost and dimensional stability. A good option in this case is the polymethylmethacrylate (PMMA), consolidated material for tissue/water equivalence (Goldstone, 1989).

Since its invention in the 1980s, three-dimensional (3D) printing techniques have been developed, matured, and used in various applications by many researchers and industrial companies worldwide. Nowadays it is revolutionizing manufacturing and many other industries with new processes and materials; especially on medical physics field, with potential production of reproducible and sophisticated phantoms (Wang et al., 2017; Filippou and Tsoumpas, 2018).

The use of 3D printing and filaments commonly found commercially for development of phantoms has been investigated (Veneziani et al., 2016; Santos et al., 2019) and research being performed on developments of quality assurance devices (OGDEN et al., 2019; Arconada-AlvarezSantiago et al., 2017), CT imaging (Hamedani et al., 2018) clinical electrons dosimetry (Diamantopoulos et al., 2018), developments of physical and anthropomorphic phantoms to mammography based on patient CT data and mathematical phantoms used for development and optimization of new breast imaging techniques, new realistic test models for X-ray breast dosimetry, as well as in development of reconstruction and image enhancing algorithms (Feradov et al.,

* Corresponding author.
E-mail address: dvillani@ipen.br (D. Villani).

https://doi.org/10.1016/j.radphyschem.2020.108728
Received 29 July 2019; Received in revised form 12 January 2020; Accepted 22 January 2020
Available online 28 January 2020
0969-806X/

2019; Daskalov et al., 2019; Esposito et al., 2019).

The application of this technique for development of low cost phantoms requires a complex study of the interaction of printed materials with different radiation types and qualities, as well as characterization of printing set-ups. Performing these measurements, it is possible to find methodologies so they can correctly mimic human tissue.

Thus, this paper aims to characterize the radiation attenuation behavior of Polylactic Acid (PLA) and Acrylonitrile Butadiene Styrene (ABS) fused filament fabrication (FFF) 3D printed phantoms and to determine the influence of different infill percentages using standard diagnostic radiology X-ray beams in comparison with PMMA solid plates and theoretical data. Study was performed to verify the 3D printed phantom use viability as an easier-handle substitute for PMMA for creation of water/tissue equivalent sophisticated phantoms.

2. Methods

2.1. Printing materials and set-ups

Phantom plates were printed using the RAISE 3D PRO2 3D printer from IPEN (Fig. 1) to determine the attenuation behavior and coefficients. For this study, plates were printed with dimensions of 80 × 80 × 1 mm^3 using +45°/-45° orientation, layer thickness (z) of 0.2 mm and variations of 100%, 95%, 80% and 50% infill. For comparison, 100 × 100 × 1 mm^3 solid PMMA plates were used as material of reference. Fig. 2 show PMMA plates used and the obtained printed phantoms. One can find the specifications (UP3D Brasil) of the 3D printing materials in Table 1.

Printing configurations were set using the ideaMAKER slicer software. Fig. 3 show the simulation of the printing of the phantom plates using rectilinear +45°/-45° orientation and Fig. 4 show the differences of the printing infill set ups.

2.2. Radiation beams and detectors

The attenuation behavior of the materials was evaluated on radiodiagnostic standard X-ray beams available from the Instrument Calibration Laboratory (LCI-IPEN) using the Pantak Seifert ISOVOLT X-ray system and the RQR beam qualities available. Phantom plates were printed and irradiated with different X-ray qualities in the diagnostic range. Details on the IEC 61267 (1994; ISO 4037-1, 1996) standards of the beams used are presented on Table 2. The attenuation coefficients were obtained experimentally for these qualities using commercial radiation detection system RaySafe with X2 R/F solid state sensor connected.

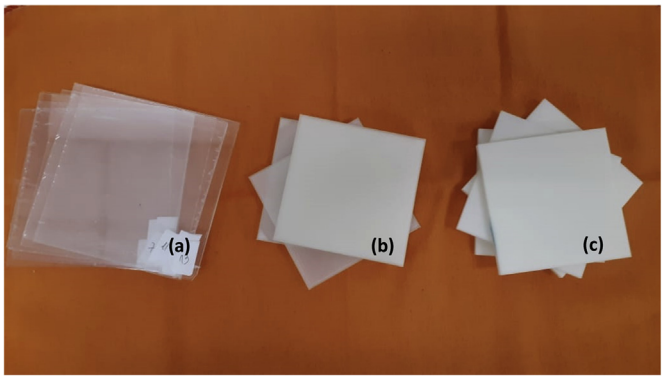

Fig. 2. PMMA (a), PLA (b) and ABS (c) phantom plates used for radiation transmission measurements.

2.3. Measurements and experimental set-up

The transmission method can be used for experimental determination of the attenuation coefficients (μ) of the materials. A simple exponential attenuation should be expected as result of the strike of the beam in a detector after passing through variable thickness absorbers. The interactions remove photons from the beam either by absorption or by scattering away from the detector and can be characterized by a fixed probability of occurrence per unit path length in the absorber. The sum of these interactions is the probability per unit path length that the photon is attenuated (Knoll, 2010; Tsoulfanidis, 2010):

$$\mu = \tau + \sigma + \kappa \quad \text{(Eq. 1)}$$

where τ is the absorption by photoelectric effect, σ Compton scattering and κ pair production.

The sample thickness was increased from zero (without attenuation) to 150 mm and positioned in front of the collimated beam exit, using the standard calibration set-up of de LCI Laboratory. The beam qualities were set adding specific filtration using the PTW filter wheel and Raysafe X2 R/F detector placed at 100 cm distance (Fig. 5). The values obtained in this procedure were analyzed using Origin® software. For each quality an exponential fit was performed in order to obtain μ of the materials, according to Eq. (2) (Knoll, 2010; Tsoulfanidis, 2010)

$$I_t = I_0 e^{-\mu t} \quad \text{(Eq. 2)}$$

where I_0 is the initial beam intensity, and I is the beam intensity when some material of thickness t is placed between radiation source and detector. Use of the linear attenuation coefficient is limited by the fact that it varies with the density of the absorber, even though the absorber

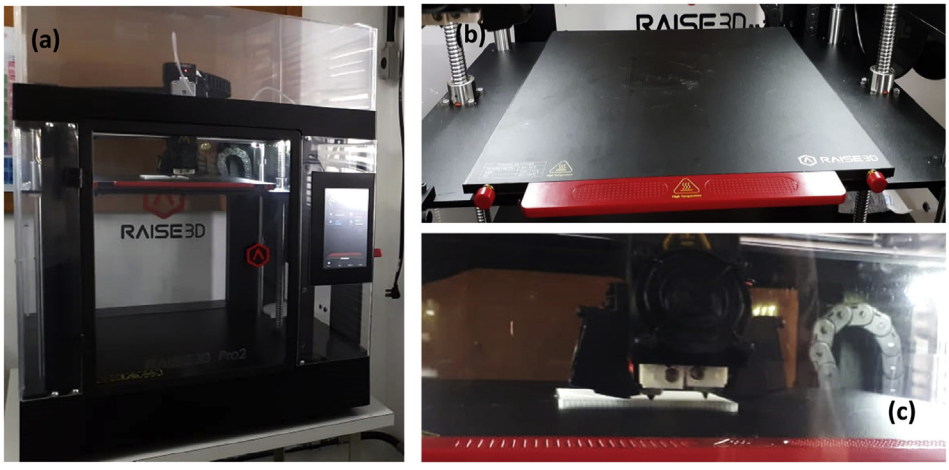

Fig. 1. RAISE 3D PRO2 printer from IPEN (a) general view (b) detail on heated bed (c) detail on extruder nozzles.

Table 1
Manufacture characteristics for PLA and ABS.

Material	Color	Nominal Density (g/cm^3)	Measured Density (g/cm^3)	Nozzle Temperature (°C)	Heated Bed Temperature (°C)	Print Speed (mm/s)
PLA	Transparent	1.24	1.1028(3)	210–220	60	50
ABS	Pure/White	1.05	0.9108(5)	240–250	105	50

material is the same and derived when beams used are monoenergetic (Knoll, 2010; Tsoulfanidis, 2010).

Measurements in this study were performed using polyenergetic X-ray filtered beams, however, for the purpose of comparing behavior between printed materials with PMMA at same experimental conditions, the transmission method is an excellent approximation since the results are relative. Once the linear attenuation coefficients are calculated, the experimental values of half-value layer (HVL) for both PMMA and printed phantoms can be calculated using Eq. 3

$$HVL = \frac{ln(2)}{\mu} \quad \text{(Eq. 3)}$$

In order to compare experimental data obtained with theoretical X-ray cross session found in the ICRU Report 44 (Goldstone, 1989) and NIST Standard Reference Database (Hubbell and Seltzer, 2004), the total mass attenuation coefficient was calculated with Eq. 4

$$\textit{total mass attenuation coefficient} = \frac{\mu}{\rho} \quad \text{(Eq. 4)}$$

where ρ is the density of the absorber.

3. Results

3.1. Radiation transmission

Fig. 6 show the experimental results on radiation transmission of 100% infill PLA and ABS plates and PMMA for the standard beams. The expected exponential behavior can be observed and applying an exponential fit to the data points, the attenuation coefficients for the different beam qualities were obtained and the results are shown in Table 3 and plotted together in Fig. 7.

When observing the coefficients obtained it is possible to perceive the differences on behavior of the transmission of the materials to the different qualities of radiation. This is a consequence of the different energies of the X-ray beams studied, characterizing attenuation energy dependence. Fig. 8 show the energy dependence on behavior of the attenuation of the materials relative to RQR 10.

The experimental results obtained for PMMA, PLA and ABS can be compared with theoretical data available at NIST database in terms of total mass attenuation. The coefficients were calculated using Eq. (4) and results compared with theoretical cross section of Muscle, PMMA and Soft Tissue, and results presented in Fig. 9.

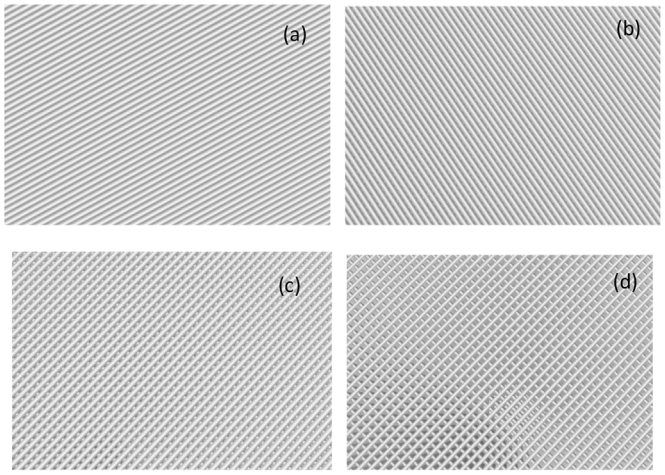

Fig. 4. Printing infill set ups simulated from ideaMAKER slice software using rectilinear +45°/-45° orientation. (a) 100% infill (b) 95% infill (c) 80% infill (d) 50% infill.

Table 2
Pantak Seifert standard beam qualities used in this study.

Beam Quality	Tube voltage (kVp)	HVL (mmAl)	Additional Filtration (mm)	Mean photon energy (keV)
RQR-2M	28	0.37	0.07Mo	15.6
RQR-4M	35	0.41	0.07Mo	16.3
RQR 3	50	1.78	2.4Al	29.7
RQR 5	70	2.58	2.8Al	34.0
RQR 8	100	3.97	3.2Al	38.1
RQR 10	150	6.57	4.2Al	46.5

3.2. HVL calculations

The HVL parameter calculated on thickness of the absorbing

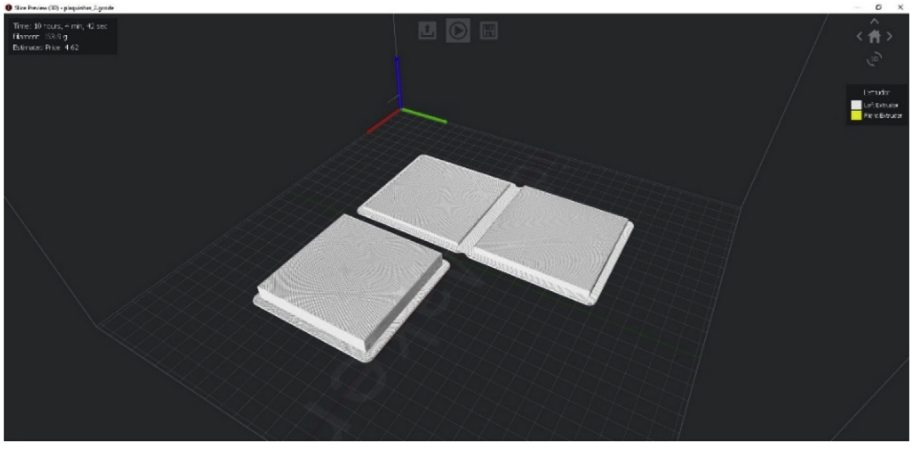

Fig. 3. ideaMAKER slicing simulation for the printing the plate phantoms.

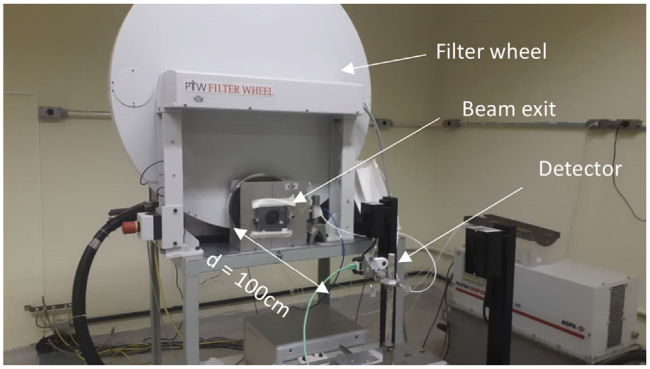

Fig. 5. Pantak Seifert irradiation set-up used in the study for irradiation of the IEC RQR standard beams.

material (PMMA, PLA, and ABS), most commonly used for radiation shielding considerations, is important to visualize in thicknesses values how much material is required to halve the beam entrance exposure. Using the attenuation coefficients (μ) of Table 3 and Eq. (3), the experimental values of HVL were calculated and one can find the results in Table 4. As a consequence of the lower attenuation results observed in Fig. 6, the HVL values for ABS plate phantoms are higher than for PMMA and printed PLA.

3.3. Infill (%) transmissions

Using the FFF 3D printing technique, decreasing the infill percentage settings reduces the material fill in the printed objects and consequently creates an air mesh inside them. When using this technique for phantom development, it is important to know the consequences of this air mesh in relation to X-ray attenuation of printed parts. Measurements of transmission of plates with less infill percentages were performed and compared with 100% infill and the results are presented in Fig. 10. As expected, the intensity of the transmitted beam increases as the infill percentage decreases, as consequence of more air and less material.

Table 3
Experimental linear attenuation coefficients obtained.

Beam Quality	μ PMMA (mm^{-1})	μ PLA (mm^{-1})	μ ABS (mm^{-1})
RQR2-M	0.113 ± 0.003	0.110 ± 0.005	0.067 ± 0.001
RQR4-M	0.108 ± 0.005	0.104 ± 0.006	0.065 ± 0.001
RQR3	0.047 ± 0.003	0.043 ± 0.003	0.030 ± 0.003
RQR5	0.042 ± 0.003	0.038 ± 0.006	0.028 ± 0.003
RQR8	0.037 ± 0.004	0.033 ± 0.005	0.025 ± 0.002
RQR10	0.031 ± 0.004	0.028 ± 0.003	0.021 ± 0.003

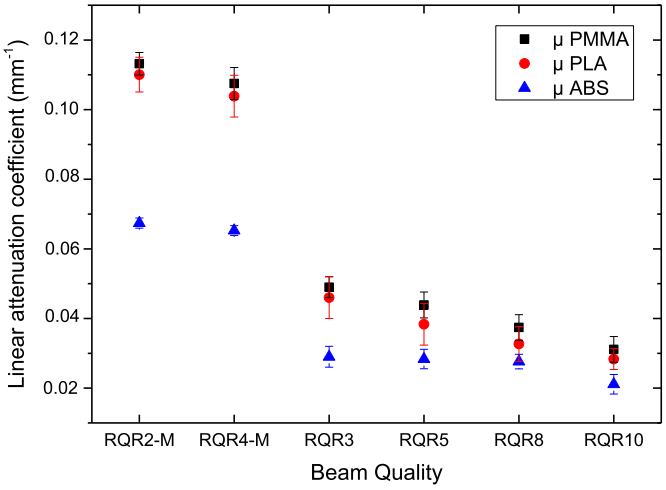

Fig. 7. Experimental attenuation coefficients obtained.

4. Discussions

Most quality control devices and phantoms, especially for dosimetry and radiation protection purposes, are completely filled either with

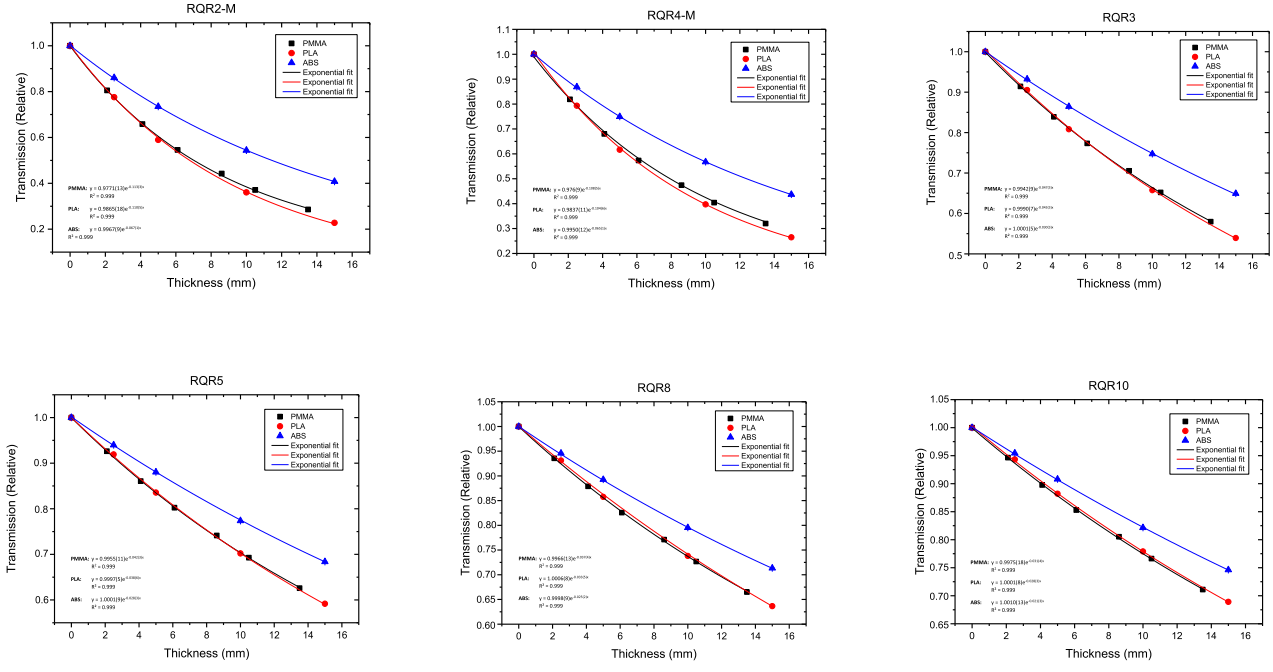

Fig. 6. Transmission data obtained with PMMA, and 100% infill PLA and ABS phantom plates for the standard beams. The error bars, when bigger than the data points, represent the standard uncertainty of tree measurements.

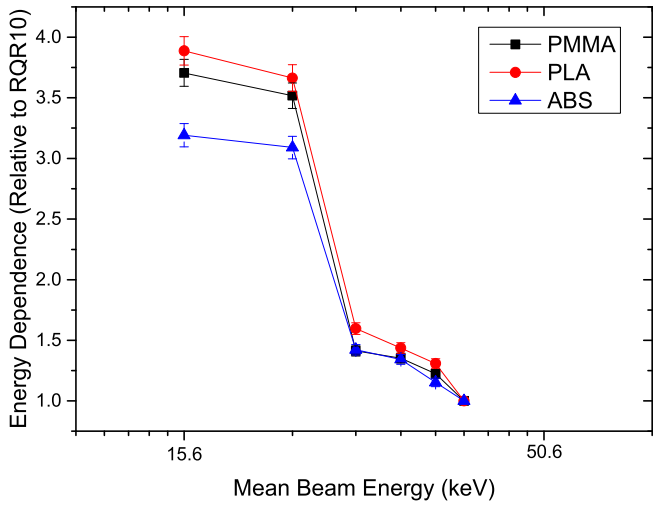

Fig. 8. Energy Dependence behavior of attenuation of materials. On the X axis the energy values for the experimental results were those of the mean beam energies presented in Table 2.

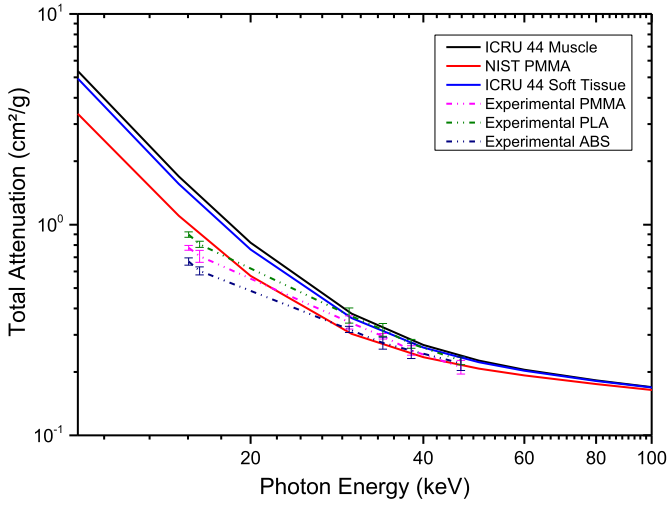

Fig. 9. Experimental total mass attenuation of PMMA, PLA and ABS compared with theoretical data of Muscle, PMMA and Soft Tissue. On the X axis the energy values for the experimental results were those of the mean beam energies presented in Table 2.

Table 4
Experimental HVL obtained for PMMA and printed materials.

Beam Quality	HVL PMMA (mm)	HVL PLA (mm)	HVL ABS (mm)
RQR2-M	6.1 ± 0.2	6.3 ± 0.3	10.3 ± 0.2
RQR4-M	6.4 ± 0.3	6.7 ± 0.4	10.7 ± 0.2
RQR3	14.7 ± 1.1	16.1 ± 1.1	24.8 ± 2.6
RQR5	16.5 ± 1.0	18.2 ± 2.8	23.1 ± 2.4
RQR8	18.7 ± 1.8	21.0 ± 3.5	27.7 ± 1.9
RQR10	24.4 ± 3.0	24.8 ± 2.2	33.0 ± 4.4

water or human tissue equivalent material. So, it is interesting to know the characteristics of 100% infill FFF 3D printed phantoms. Analyzing the experimental transmission results one can observe that the standard beams are slightly more attenuated with PMMA than PLA and yet both presented statistically equivalent behavior within 1σ (Fig. 7). Results obtained with ABS, despite lower attenuation coefficients, have reported statistical equivalency for both RQR2-M and RQR4-M beams and for RQR3, RQR5 and RQR8 beams.

The imaging X-ray qualities used in this work range from low energy

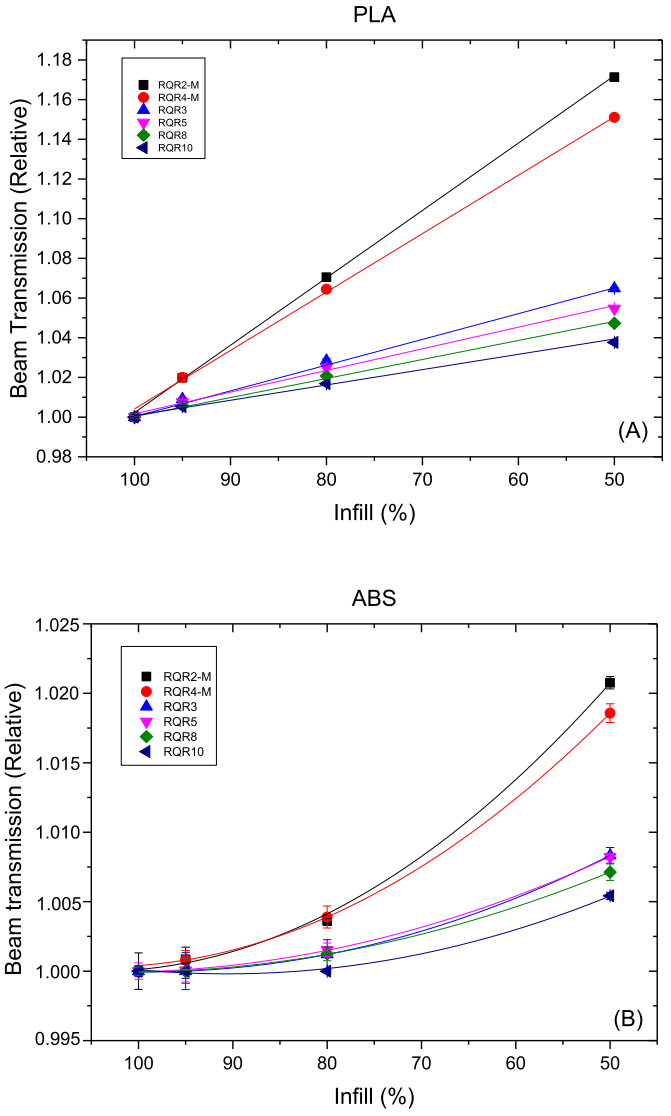

Fig. 10. Transmission behavior for PLA and ABS printed phantoms with different infill percentages (relative to 100%).

photons used in mammography (~15.6 keV of mean energy), where photoelectric effect prevails, to slightly higher energy beams used in radiodiagnostic (~45.6 keV of mean energy) where there is a significant increase in Compton scattering. Thus, it is possible to observe that differences on μ for each material relates on beam energy and the approximation used sum both interactions. Results on Fig. 8 show that PMMA and PLA attenuates ~4 times more RQR2-M beams when compared to RQR10 and it is expected that for energetic radiation beams will reduce the attenuation differences of the materials. This effect on energy also causes the increased material thickness required to reach the Half-value layers, as observed in Table 4.

Comparison of the experimental total attenuation coefficients with the theoretical NIST data presented in Fig. 9. The attenuation values for PMMA and printed PLA are also statistically equivalent within 1σ for all beam qualities studied; with the ABS getting closer in equivalence as the beams become more energetic. Note that the experimental data values are an approximation to the theoretical values, since the measurements were performed using filtered polyenergetic beams. The beams are likely to harden by increasing the thickness of attenuators during measurements, but the results are nonetheless consistent with the theoretical data.

There is considerable difference between experimental and

theoretical data for the RQR2-M and RQR4-M qualities. This effect most likely be due to the fact that the X2 R/F dosimetric probe used for the measurements suffers efficiency effects when dealing with lower energy beams used in mammography (Raysafe X2 R/F). At the same time, by analyzing the experimental data within themselves, there is consistency between PMMA attenuations in relation to PLA and ABS.

In the characterization of printed phantoms, it is necessary to evaluate the impact that different infill percentages have on the radiation transmission. As expected, Fig. 10A and B shows that the less absorbing material is present, more beam is transmitted. Ranging from 100% down to 50% infill, PLA phantoms presented up to ~16% less attenuation and a linear function can be fitted on the experimental data. ABS presented second degree polynomial behavior for the same conditions, but with less significant attenuation depletion, with differences in order of 2.5% between 50 and 100% infill. These information can be useful, as reported by Hamedani et al. (2018), who used infill variations of 10 and 20% to control radiopacity in the construction of a 3D printed pelvis simulator for CT imaging.

5. Conclusions

This paper reports the behavior of two commercial 3D printing filaments on standard X-ray beams and the use the fused filament fabrication (FFF) with different set-ups. PMMA measurements were also performed as reference and all results compared with theoretical data. Attenuation characteristics evaluated indicates the suitable equivalence of PLA to PMMA for 3D printing water/tissue equivalent most complex geometry phantoms. ABS can as well be used to mimetize less dense structures especially when considering more energetic beams. The infill differences can also be used in this manner. Considering the characteristics of the X-ray beams used in this study, experimental results are coherent with theoretical data. Different printing modes characterized together with their attenuation coefficients for the X-ray standard beams studied can lead further developments of new 3D printed phantoms in our institute in a cheaper way.

CRediT authorship contribution statement

D. Villani: Formal analysis, Data curation, Writing - review & editing. **O. Rodrigues:** Formal analysis, Data curation, Writing - review & editing. **L.L. Campos:** Supervision, Writing - review & editing.

Declaration of competing interest

The authors declare that there is no conflict of interests regarding the publication of this paper.

Acknowledgments

The authors would like to thank Fundação de Amparo à Pesquisa do Estado de S. Paulo - FAPESP (process number 2017/50332-0), Conselho Nacional de Desenvolvimento Científico e Tecnológico - CNPq (process number 142098/2017-5) and Coordenação de Aperfeiçoamento de Pessoal de Nível Superior - CAPES (process number 554/2018) for the financial support and the organization committee of ICDA3.

Appendix A. Supplementary data

Supplementary data to this article can be found online at https://doi.org/10.1016/j.radphyschem.2020.108728.

References

Arconada-Alvarez, Santiago J., et al., 2017. The development and characterization of a novel yet simple 3D printed tool to facilitate phantom imaging of photoacoustic contrast agents. Photoacoustics 5, 17–24.
Daskalov, Sivo, et al., 2019. Anthropomorphic physical breast phantom based on patient breast CT data: preliminary results. In: Mediterranean Conference on Medical and Biological Engineering and Computing. Springer, Cham, pp. 367–374.
Dewerd, Larry A., 2014. The Phantoms of Medical and Health Physics. Springer, Berlin.
Diamantopoulos, S., et al., 2018. Theoretical and experimental determination of scaling factors in electron dosimetry for 3D-printed polylactic acid. Med. Phys. 45 (4), 1708–1714.
Esposito, G., et al., 2019. Investigation of the refractive index decrement of 3D printing materials for manufacturing breast phantoms for phase contrast imaging. Phys. Med. Biol. 64 (7), 075008.
Feradov, Firgan, Marinov, Stoyko, Bliznakova, Kristina, 2019. Physical breast phantom dedicated for mammography studies. In: Mediterranean Conference on Medical and Biological Engineering and Computing. Springer, Cham, pp. 344–352.
Filippou, V., Tsoumpas, C., 2018. Recent advances on the development of phantoms using 3D printing for imaging with CT, MRI, PET, SPECT, and ultrasound. Med. Phys. 45 (9), e740–e760.
Goldstone, K.E., 1989. Tissue substitutes in radiation dosimetry and measurement. In: ICRU Report 44, International Commission on Radiation Units and Measurements, USA, pp. 1990.
Hamedani, B.A., et al., 2018. Three-dimensional printing CT-derived objects with controllable radiopacity. J. Appl. Clin. Med. Phys. 19 (2), 317–328.
Hubbell, J.H., Seltzer, S.M., 2004. X-ray mass attenuation coefficients. NIST Standard Reference Database 126 2019.
IEC 61267, International Electrotechnical Commission, et al., 1994). Medical Diagnostic X-ray Equipment-Radiation Conditions for Use in the Determination of Characteristics.
International Atomic Energy Agency, 2007. Dosimetry in Diagnostic Radiology: an International Code of Practice. IAEA, Vienna (Technical Report Series No. 457).
ISO 4037-1, 1996. X and Gamma Reference Radiation for Calibrating Dosemeters and Doserate Meters and for Determining Their Response as a Function of Photon Energy - Part 1: Radiation Characteristics and Production Methods.
Knoll, Glenn F., 2010. Radiation Detection and Measurement, fourth ed. John Wiley & Sons.
Ogden, K.M., Morabito, K.E., Depew, P.K., 2019. 3D printed testing aids for radiographic quality control. J. Appl. Clin. Med. Phys. 20 (5), 127–134.
Raysafe X2 R/F user manual. Available in: http://mediabank.raysafe.com/downloadAsset.jsp?catalog=RaySafe+Media+Bank&id=2704&.
Santos, J.C., et al., 2019. Characterization and applicability of low-density materials for making 3D physical anthropomorphic breast phantoms. Radiat. Phys. Chem. 108361.
Tsoulfanidis, Nicholas, 2010. Measurement and Detection of Radiation. CRC press.
UP3D Brasil PLA and ABS filaments manufacture. Available in. https://www.up3dbrasil.com.br/.
Veneziani, G.R., et al., 2016. Attenuation coefficient determination of printed ABS and PLA samples in diagnostic radiology standard beams. In: Journal of Physics: Conference Series. IOP Publishing, 012088.
Wang, Kan, et al., 2017. A review on the 3D printing of functional structures for medical phantoms and regenerated tissue and organ applications. Engineering 3 (5), 653–662.